Supporting Information

Giant spontaneous polarization for enhanced ferroelectric property of biaxially oriented poly(vinylidene fluoride) by mobile oriented amorphous fractions

Guanchun Rui,[1,#] Yanfei Huang,[2,#] Xinyue Chen,[1] Ruipeng Li,[3] Dingrui Wang,[4] Toshikazu Miyoshi,[4] Lei Zhu[1,*]

[1] *Department of Macromolecular Science and Engineering, Case Western Reserve University, Cleveland, Ohio 44106-7202, United States*
[2] *College of Materials Science and Engineering, Shenzhen Key Laboratory of Polymer Science and Technology, Shenzhen University, Shenzhen 518055, P. R. China*
[3] *National Synchrotron Light Source II, Brookhaven National Laboratory, Upton, New York 11973, United States*
[4] *Department of Polymer Science, University of Akron, Akron, Ohio 44325-3909, United States*

[#] These authors contribute equally to this work.

* Corresponding author. Email: lxz121@case.edu (L. Zhu)

I. Electric Poling of the Fresh BOPVDF at 500 MV/m for 100 Times

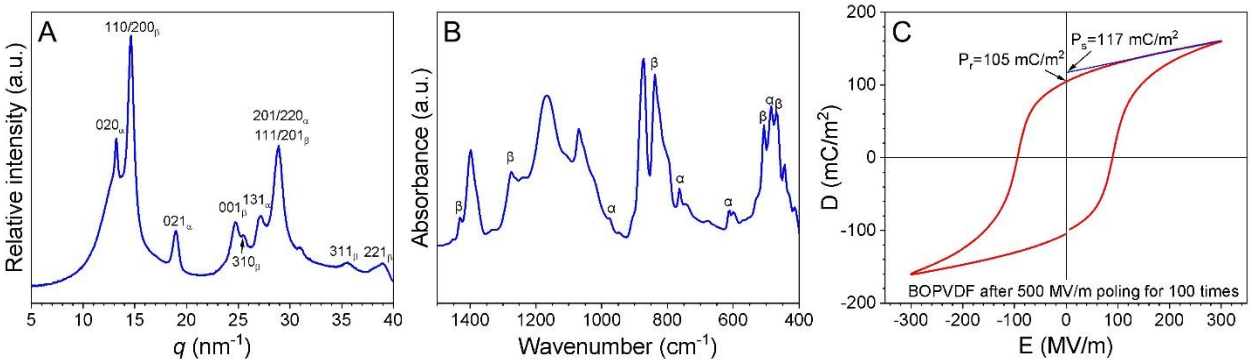

Fig. S1. (A) 1D XRD, (B) FTIR, and (C) bipolar D-E loops for the BOPVDF unidirectionally poled at 500 MV/m for 100 times. The poling electric field has a unidirectional sinusoidal waveform at 10 Hz (room temperature). From the FTIR spectrum in (B), the contents of α and β crystal are determined to be ca. 20% and 80%, respectively.[S1]

II. WAXD Crystallinity Calculation for the Poled BOPVDF

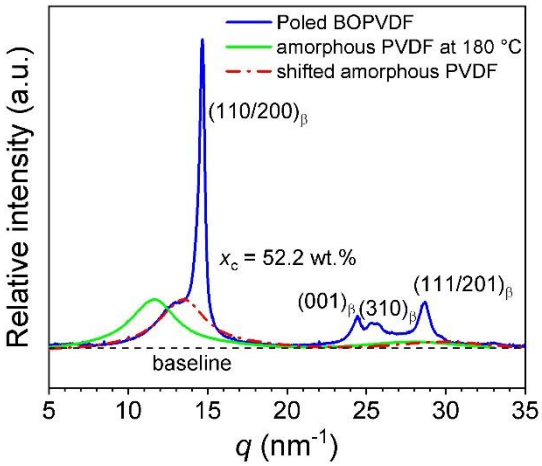

Fig. S2. 1D WAXD profiles for the highly poled BOPVDF film at room temperature and the molten PVDF at 180 °C.

Crystallinity (x_c) was calculated by the 1D WAXD method. Fig. S2 shows the 1D WAXD profiles for the highly poled BOPVDF film at room temperature (the blue curve) and the molten PVDF at 180 °C (the green curve). It is seen that the strongest amorphous halo for the molten PVDF centered at 11.7 nm^{-1}, corresponding to an average interchain distance of 0.537 nm. This amorphous halo did not match with the amorphous halo of the poled BOPVDF, which appeared at 13.2 nm^{-1} (i.e., 0.476 nm). The larger average spacing of the amorphous halo in the molten PVDF could not be attributed to the thermal expansion, because the calculated linear thermal expansion coefficient was too high [~1.0×10^{-3} /K, much higher than that of water (7×10^{-5} /K)]. Instead, it should be attributed the presence of significant OAF in BOPVDF, which had a smaller interchain spacing than in the IAF. To fit the amorphous halo of the poled BOPVDF, the green curve was right-shifted; see the red curve. After peak-integration, the crystallinity was calculated to be 0.52, which is similar to the x_c of 0.54 obtained by DSC for the fresh BOPVDF, as we reported before.[S2]

III. Subtraction of AC Electronic Conduction for the D-E Loops of the Poled BOPVDF

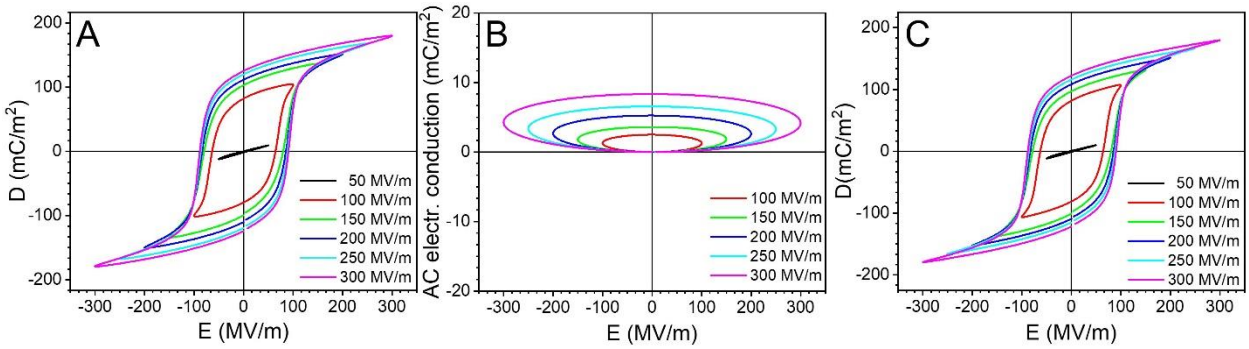

Fig. S3. (A) Raw-data bipolar D-E loops, (B) AC electronic conduction loops, and (C) final bipolar D-E loops at room temperature, after subtraction of AC electronic conduction from the raw-data D-E loops. The poling electric fields have a sinusoidal waveform at 10 Hz.

IV. Extrapolation of Dielectric Constant to Low Temperatures for the Molten PVDF

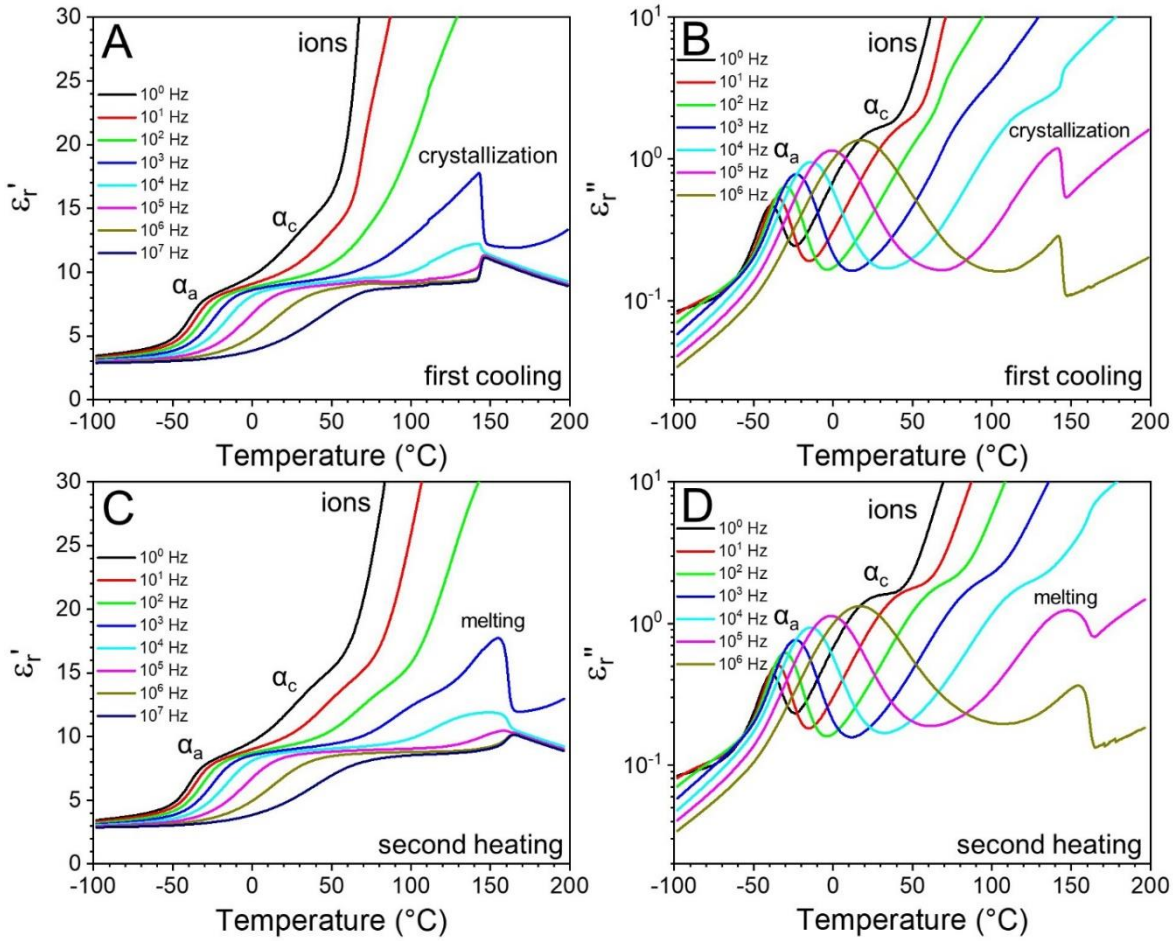

Fig. S4. Temperature-scan BDS results of (A,C) ε_r' and (B,D) ε_r'' under different frequencies for (A,B) the first cooling and (C,D) the second heating processes for the MR PVDF. The α_a, α_c, impurity ion conduction, crystallization, and melting processes are labeled in the plots.

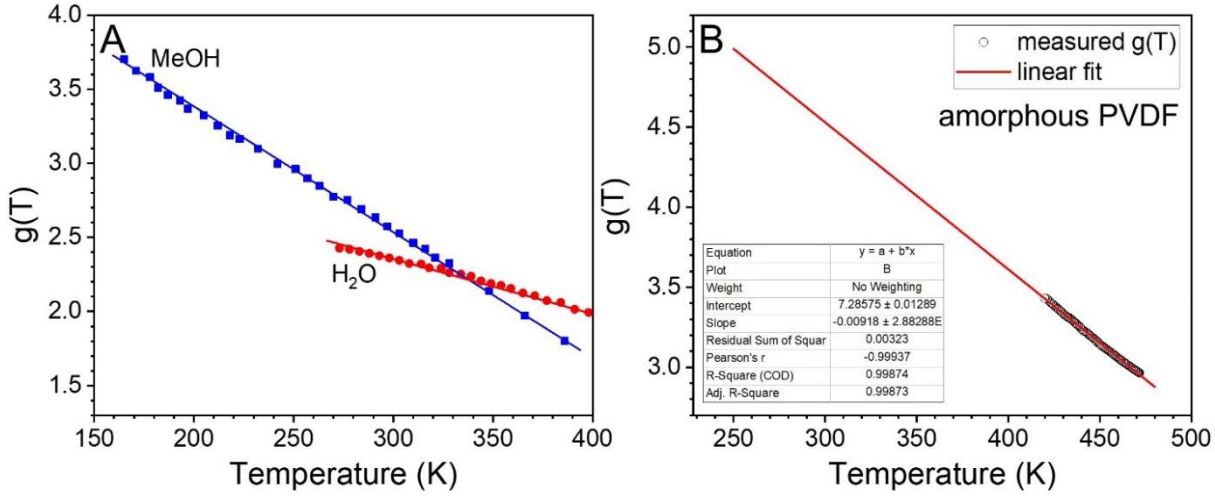

Fig. S5. The correlation g-factor, g(T), as a function of temperature for (A) methanol and water, and (B) molten PVDF.

For the molten PVDF, the dielectric constant was measured by BDS during cooling between 145 and 200 °C (see Fig. S4A). Using the Kirkwook-Fröhlich equation, we can obtain the correlation g-factor, g(T), as a function of temperature:[S3]

$$\frac{(\varepsilon_{rs}-\varepsilon_{r\infty})(2\varepsilon_{rs}+\varepsilon_{r\infty})}{\varepsilon_{rs}(\varepsilon_{r\infty}+2)} = \frac{N_A \rho g(T) \mu^2}{9\varepsilon_0 MkT} \qquad \text{(S1)}$$

where ε_{rs} and $\varepsilon_{r\infty}$ are relative static and high-frequency (including only electronic and atomic polarizations) dielectric constants, N_A the Avogadro's number, ρ density, μ dipole moment, ε_0 vacuum permittivity, M molecular weight, *k* Boltzmann constant, T temperature. For this analysis, most parameters are taken from our previous publication.[S2] For molten PVDF, $\varepsilon_{r\infty}$ = 2.2, ρ = 1.680 g/cm^3, μ = 0.923 D, M = 64 g/mol. Similarly, we also calculate the g-factor for water and methanol, using their dielectric constants at different temperatures.[S4] For water, we use the following parameters: $\varepsilon_{r\infty}$ = 2.09 (calculated from Clausius-Mossotti equation,[S3] given the refractive index *n* = 1.333), ρ = 0.997 g/cm^3, μ = 1.855 D (vapor phase), M = 18 g/mol. For methanol, we use the following parameters: $\varepsilon_{r\infty}$ = 2.07 (calculated from Clausius-Mossotti equation, given the refractive index *n* = 1.326), ρ = 0.792 g/cm^3, μ = 1.70 D (vapor phase), M = 32 g/mol. Fig. S5A shows the g(T) as a function of temperature for water and methanol, and g(T) has a simple linear relationship with temperature. For molten PVDF, we also assume a linear relationship between g(T) and T (Fig. S5B). By extrapolating to 250 K, g(T) was obtained for temperature below the crystallization temperature (ca. 430 K). Using the extrapolated g(T) values and Eqn. (S1), the ε_{rs} can be calculated, as shown in Fig. 9 in the main text.

V. Nonlinear Harmonics D_n^* (n = 1-3) for the Poled BOPVDF Film

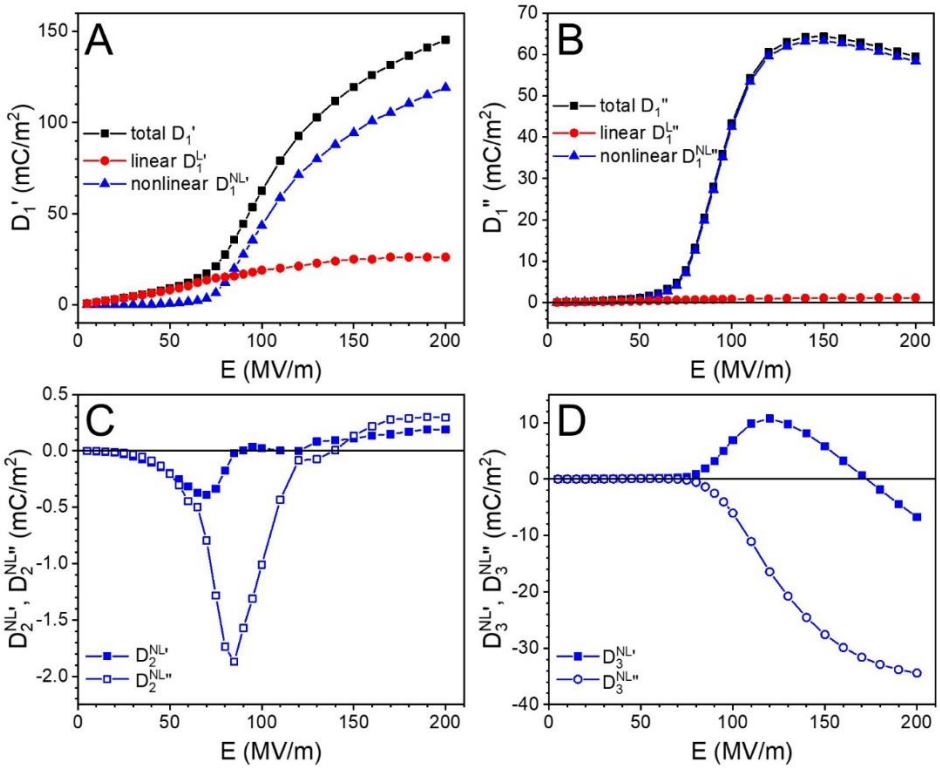

Fig. S6. Nonlinear harmonics (A) D_1', (B) D_1'', (C) $D_2^{NL\prime}/D_2^{NL\prime\prime}$, and (D) $D_3^{NL\prime}/D_3^{NL\prime\prime}$ for the poled BOPVDF film at room temperature.

VI. Nonlinear Dielectric and Ferroelectric Properties for the 120 °C-annealed Poled BOPVDF

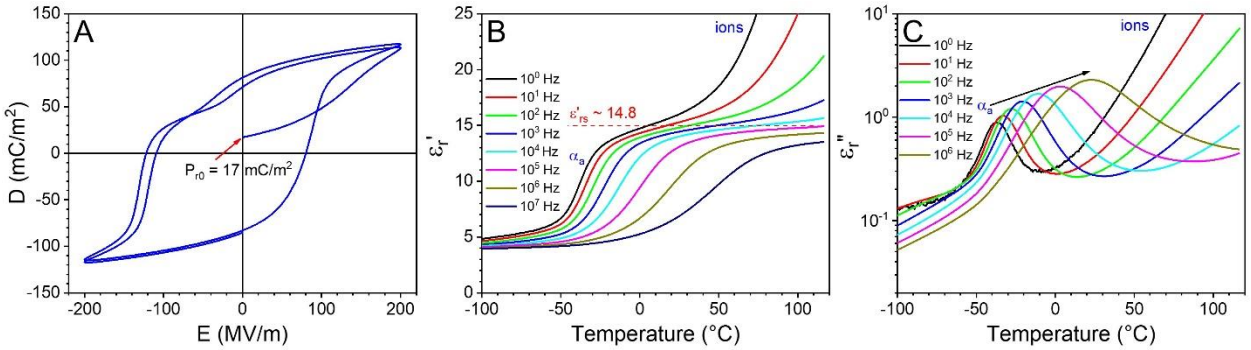

Fig. S7. (A) The first two continuous bipolar D-E loops for the poled BOPVDF film after thermal annealing at 120 °C for 4 days. Temperature-scan BDS results (B) ε_r' and (C) ε_r'' under different frequencies for the 120 °C-annealed poled BOPVDF film.

We annealed the poled BOPVDF film at 120 °C for 4 days. The annealing temperature should be chosen that it was high enough to depolarize the sample as much as possible, but no crystal-melting should take place, because melt-recrystallization could lead to the formation of nonpolar α crystals. Indeed, the FTIR result showed that no any α crystals were observed for the sample after thermal annealing at 120 °C for 4 days (see Fig. 2B). As shown in the first two bipolar D-E

loops in Fig. S7A, the P_{r0} after thermal annealing at 120 °C for 4 days was determined to be 17 mC/m^2. Obviously, the P_{r0} largely diminished for the 120 °C-annealed poled BOPVDF film, which still contained 100% β crystals. However, it would not decrease zero, consistent with a previous report.[S5] It is likely that the chain-packing in the β crystals would become tighter upon thermal annealing, which prevented complete randomization of the aligned ferroelectric domains. Note that the E_c values in the negative branches were higher than those in the positive branches. Similar phenomenon was also observed for thermally annealed poled nylon-11.[S6] This can be attributed to the well-annealed, positively aligned large ferroelectric domains, which are more difficult to be switched to the negative direction with a high $-E_c$. Once some domains were switched to the negative direction, the well-annealed crystalline and domain structures were disrupted, and they became easier to be switched back to the positive direction with a lower $+E_c$.

The dielectric property of the 120 °C-annealed poled BOPVDF film was studied by temperature-scan BDS. The results in Figs. S7B,C were similar to those of the poled BOPVDF film in Figs. 3E,H, except that the ε_{rs}^{a} became smaller, only 14.8. Using Eqns. (4) and (5) in the main text, the ε_{rs}^{OAF} for the 120 °C-annealed poled BOPVDF film was also calculated. Actually, it was between those of the highly poled (100% β crystals) and the fresh BOPVDF (70% α and 30% β crystals). This result indicated that the OAF in the β PVDF behaved differently from that in the α PVDF, largely due to the different chain conformations in the β and α crystals. In addition, the large internal electric field in the macroscopically poled BOPVDF sample also influenced the dielectric behavior of the OAF.

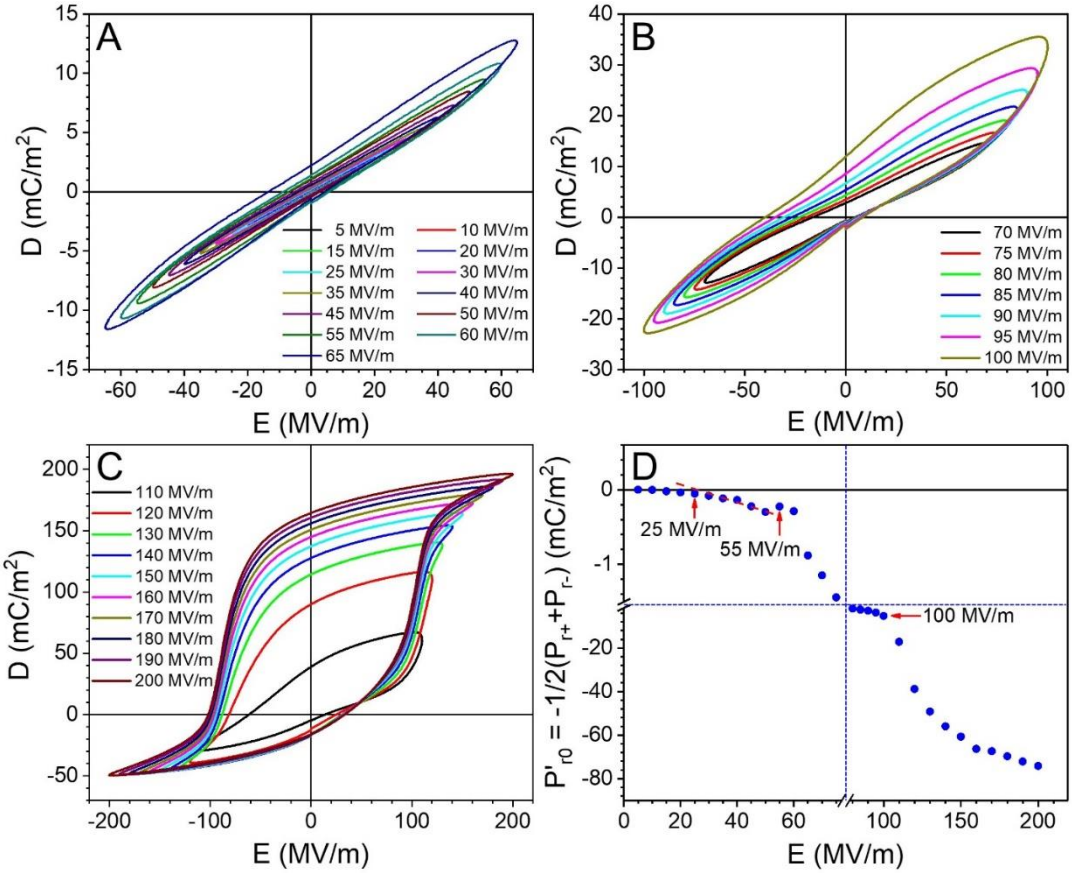

Fig. S8. Bipolar D-E loops for the 120 °C-annealed poled BOPVDF film at room temperature, when the poling field is (A) 5-65 MV/m, (B) 70-100 MV/m, and (C) 110-200 MV/m. (D) The apparent P'_{r0} as a function of the poling electric field at room temperature. The poling electric field has a sinusoidal waveform at 10 Hz, and the second loop is presented here to avoid the transient effect at the beginning of poling.

The ferroelectric property of the 120 °C-annealed poled BOPVDF film was studied by progressive bipolar D-E loops. Figs. S8A,B,C show the second loops at 5-65, 70-100, and 110-200 MV/m, respectively. Different from the poled BOPVDF film, the D-E loops for the 120 °C-annealed film appeared to be symmetric when the poling field was below 60 MV/m (Fig. S8A). This is consistent with the fact that the P_{r0} in this sample was relatively small (17 mC/m^2). When the poling field increased to 65 MV/m and above, the loops became broader in the positive half (Fig. S8B). This is attributed to the negative ferroelectric domains from the previous bipolar poling. With further increasing the poling field above 150 MV/m, the loops became more symmetric, but having a significant negative P_{r0} from the previous bipolar poling (Fig. S8C). Fig. S8D shows the apparent P'_{r0} during the progressive bipolar poling. Above 25 MV/m, a finite (negative) P'_{r0} started to appear. This is different from the poled BOPVDF film, which exhibited a positive P'_{r0} for the poling field <80 MV/m (Fig. 10D). At 55 MV/m, there was a discontinuity in the trend, indicating the onset of ferroelectric switching of certain β crystals. After that, a substantial increase in the $|P'_{r0}|$ started to appear. Eventually, the E_c was seen at 100 MV/m. Compared with the highly poled BOPVDF, the onset of ferroelectric switching for the OAF and the β crystals in the 120 °C-annealed poled BOPVDF film appeared at slightly lower electric fields, whereas the E_c appeared at a higher electric field.

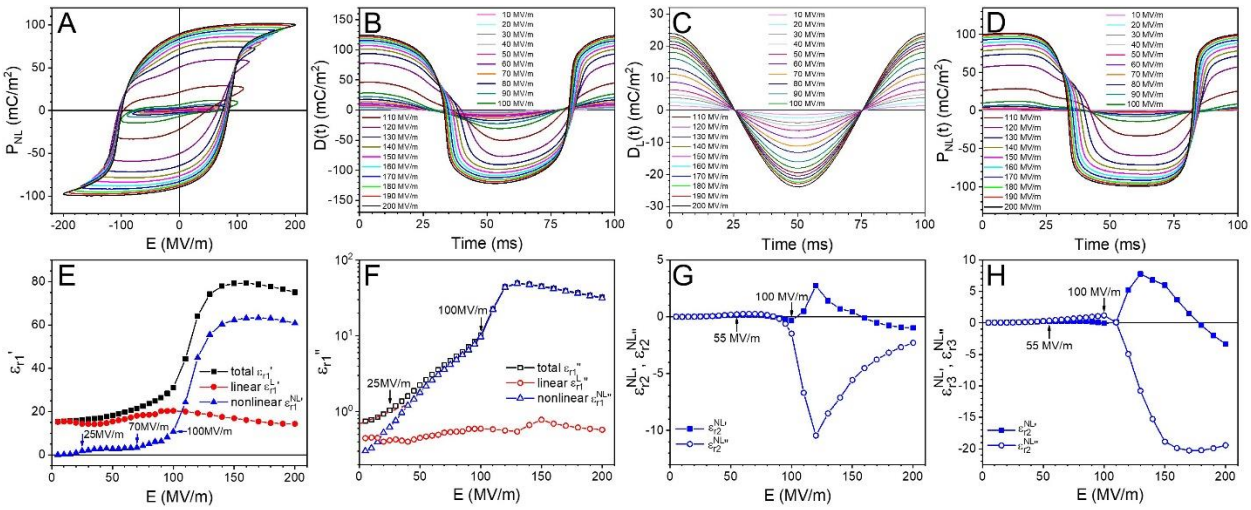

Fig. S9. (A) P_{NL}-E loops for the 120 °C-annealed poled BOPVDF at room temperature after subtraction of the D_{def} from the centered bipolar D-E loops in Fig. S8. (B) Total, (C) linear, and (D) nonlinear D(t) waves for the 120 °C-annealed poled BOPVDF film. After Fourier transform, (E) ε_{r1}', (F) ε_{r1}'', (G) $\varepsilon_{r2}'/\varepsilon_{r2}''$, and (H) $\varepsilon_{r3}'/\varepsilon_{r3}''$ are obtained for the poled BOPVDF film at room temperature.

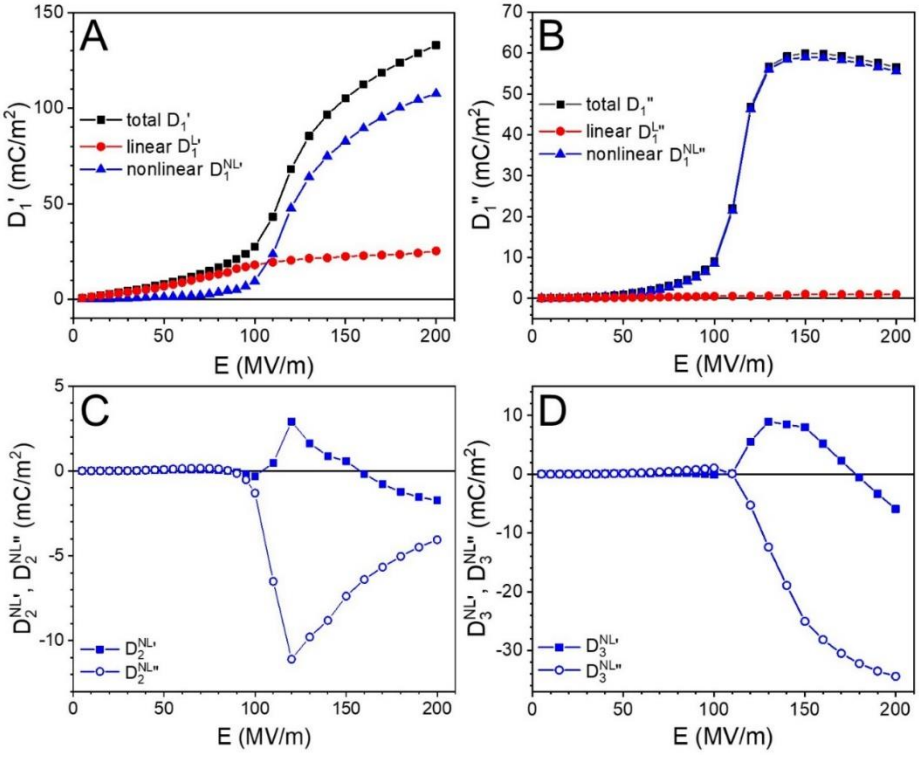

Fig. S10. Nonlinear harmonics (A) D_1', (B) D_1'', (C) $D_2^{NL\prime}/D_2^{NL\prime\prime}$, and (D) $D_3^{NL\prime}/D_3^{NL\prime\prime}$ for the 120 °C-annealed poled BOPVDF film at room temperature.

The ferroelectric property was quantified by the nonlinear dielectric constant analysis. After subtraction of the D_{def}, the P_{NL}-E loops were obtained, as shown in Fig. S9A. The total D(t), the linear $D_L(t)$, and the nonlinear $P_{NL}(t)$ waves are shown in Figs. S9B,C,D, respectively, from which

the D_n* components were obtained in Fig. S10. The total, linear, and nonlinear ε_{r1}' and ε_{r1}'' are given in Figs. S9E,F. The $\varepsilon_{r1}^{NL\prime}$ exhibited two increases at 25 and 70 MV/m, corresponding to the onset of ferroelectric switching of the OAF and the β crystals, respectively. Above 100 MV/m, the $\varepsilon_{r1}^{NL\prime}$ significantly increased, corresponding to the E_c. Similarly, the total ε_{r1}'' also exhibited a slope change at 25 MV/m and the E_c at 100 MV/m. The nonlinear $\varepsilon_{r2}^{NL\prime}/\varepsilon_{r2}^{NL\prime\prime}$ and $\varepsilon_{r3}^{NL\prime}/\varepsilon_{r3}^{NL\prime\prime}$ were nearly zero below 50 MV/m, above which finite values were seen (Figs. S9G,H). Again, the E_c was observed around 100 MV/m in these plots.

VII. Determination of Nonlinear Harmonics D_n* (n = 1-3) for the SC P(VDF-HFP) Film

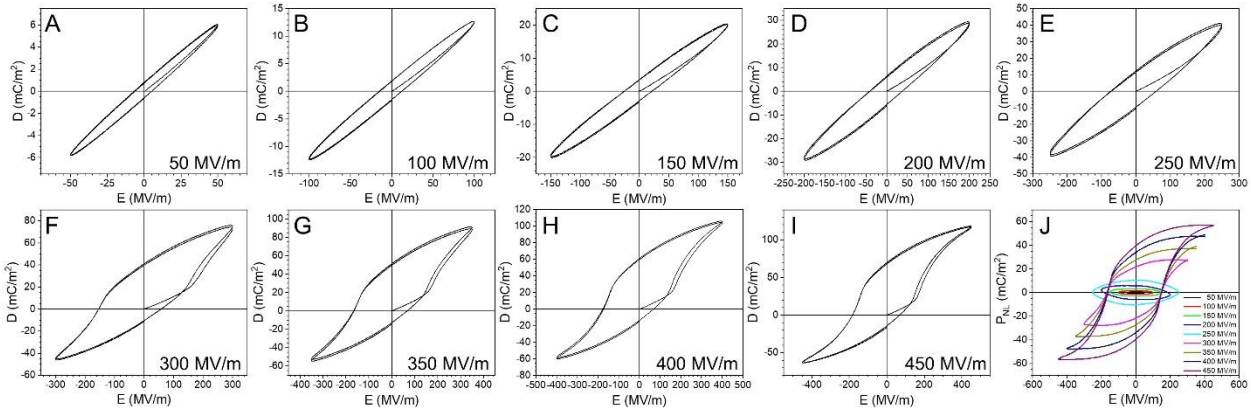

Fig. S11. (A-I) First two continuous bipolar D-E loops for the SC P(VDF-HFP) film under different poling fields at room temperature. (J) P_{NL}-E loops after subtraction of the D_{def} from the second bipolar loops in (A-I).

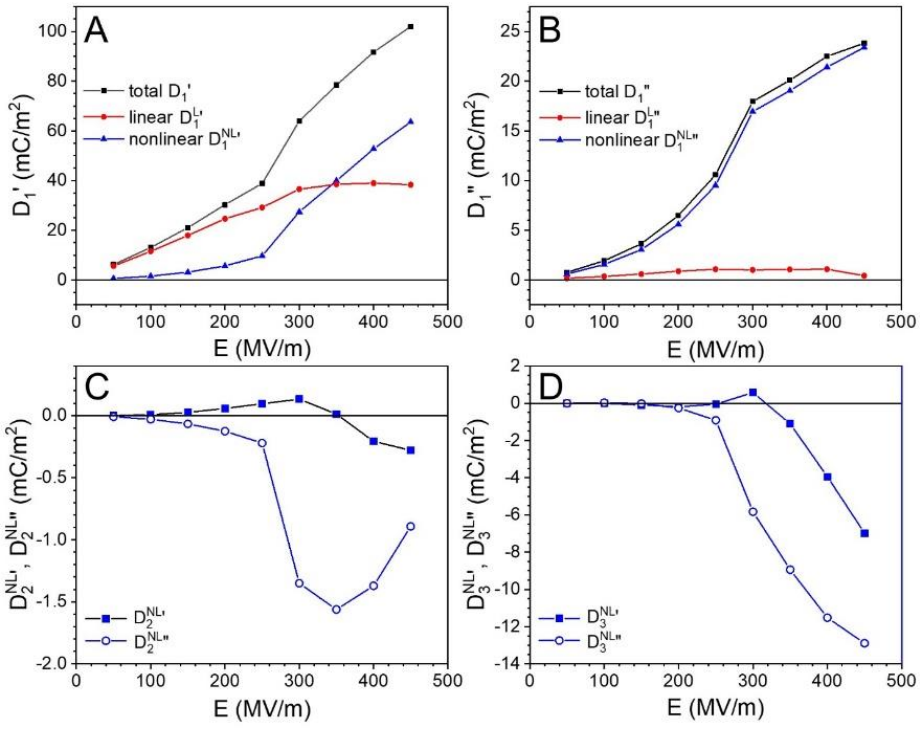

Fig. S12. Nonlinear harmonics (A) D_1', (B) D_1'', (C) $D_2^{NL\prime}/D_2^{NL\prime\prime}$, and (D) $D_3^{NL\prime}/D_3^{NL\prime\prime}$ for the SC P(VDF-HFP) film at room temperature.

References

S1. X. Cai, T. Lei, D. Sun, and L. Lin, *RSC Adv.* 2017, **7,** 15382-15389.

S2. L. Yang, J. Ho, E. Allahyarov, R. Mu, and L. Zhu, *ACS Appl. Mater. Interfaces*, 2015, **7,** 19894-19905.

S3. K. C. Kao, *Dielectric Phenomena in Solids: with Emphasis on Physical Concepts of Electronic Processes*, Elsevier Academic Press, Boston, 2004.

S4. B. Maribo-Mogensen, G. M. Kontogeorgis, and K. Thomsen, *J. Phys. Chem. B,* 2013, **117,** 3389-3397.

S5. M. P. Silva, C. M. Costa, V. Sencadas, A. J. Paleo, and S. Lanceros-Méndez, *J. Polym. Res.,* 2011, 18, 1451-1457.

S6. Z. Zhang, M. Litt, and L. Zhu, *Macromolecules,* 2017, **50,** 5816-5829.